Site Torsional Motion and Dispersive Excitation Hopping Transfer in π-Conjugated Polymers†

K. Brunner,‡ A. Tortschanoff,‡ Ch. Warmuth,‡ H. Bässler,§ and H. F. Kauffmann*,‡

Institut für Physikalische Chemie der Universität Wien, Währingerstrasse 42, A-1090 Wien, Austria, and Institut für Physikalische Chemie, Kernchemie und Makromolekulare Chemie, Philipps-Universität, D-35032 Marburg, Germany

Received: August 30, 1999

Photoexcitations coupled to intrachain, backbone modes of a flexible π-conjugated polyarylene polymer and their effect on the relaxational dynamics of migrative excitation transfer have been examined by using femtosecond and picosecond time resolved fluorescence techniques. In poly[4,4′-diphenylene-1,2-di(3,4-dimethoxyphenyl)vinylene], DMOP-PDPV, a vertical excitation into the biphenylic segmental unit is subject to a quasi-instantaneous torsional, energetic relaxation that gives rise to large bathochromic shift of the gated fluorescence spectrum on time scales < 200 fs. For times > 200 fs the (new-equilibrium) excited-state population evolves in the subsequent, electronic excitation energy transfer process (EET), but the rates in the ongoing, dissipative energy relaxation (up to several tens of nanoseconds!) are relatively slow and significantly delayed as compared to those in the more rigid poly(phenylenevinylene), PPV. The results are interpreted in terms of factored time scales for nuclear motion and electronic hopping modes. The significant slowing of the EET is related to the reduced Förster spectroscopic overlap integral, as a result of the *sudden* (<200 fs), large Stokes shift between vertical and structurally relaxed excitations. The energy shift of fluorescence photons in the course of EET, comparatively smaller than that brought about by the nuclear relaxation process and, due to the deceleration of EET, even still detectable on a nanosecond scale, can be understood as the result of a dissipative relaxation along a site energy cascade. The latter energy-dispersive pathway stems from a density of states (DOS) of localized S_1-states whose incoherent electronic communication can be adequately described within the framework of a molecular, excitonic picture in the limit of incoherent, non-Markovian motion.

I. Introduction

The pathways of generation and relaxation of optical, elementary excitations in π-conjugated main-chain polymers have been a topic of vivid debate over the past decade. In particular, for the poly(phenylenevinylene), PPV, and its substitutional derivatives, a great deal of activity has been focused on the excited-state dynamics of these systems,[1−4] since answers to these fundamental questions have also an enormous impact on the research and development of novel, molecular materials in optoelectronic and photonic applications. In these polychromophoric systems the predominant photophysical events are controlled by intersite processes of electronic coupling and nuclear motion in typical many-body interactions, so the macroscopic optical response is a complex convolution of microscopic coherent/incoherent evolutions. In the past PPV has been considered to be a one-dimensional semiconductor tractable by the SSH-Hamiltonian[5] that takes into account neither Coulomb nor electron correlation effects, but assumes local electron−phonon coupling larger than intersite coupling. In this picture the initial band-to-band excitation corresponds to free electron−hole pairs that suddenly undergo self-localization and energy stabilization to form a polaron and recombination fluorescence, in a second step. Accordingly the slight red shift of the fluorescence may be indicative of the energy of polaron formation due to the structural relaxation process of the initial excitation.[6,7]

A model that describes more realistically the PPV chain rests upon the statistical conformational disorder.[1,3] Accordingly, this approach predicts a collection of weak-to-strong, conformational breaks that give rise to a variation of conjugation lengths, i.e., an ensemble of segmental chain units distributed in length and self-energy, and to the formation of a density of states (DOS) of S_1-levels upon excitation. The excitation is associated with strong electron−hole correlation, delocalized over distinct lengths of the molecular segmental subunits (sites) and dressed by some structural relaxation. However, it is highly localized with regard to the physical length of the main-chain backbone and is still capable of migrating along the site-to-site architecture of the chain. As a consequence, for time scales longer than the inverse dephasing, the optical dynamics in PPV-type polymers is governed by polaronic miniexcitons, i.e., Coulomb-bound electron−hole pairs[8,9] in typically energy-dispersive, incoherent excitation transfer events driven by the dissipative energy relaxation toward the tail and bottom states of the DOS. Numerous results based on site-selective fluorescence measurements,[10] electroabsorption measurements,[3] and stimulated emission pump−probe studies[11] have established this so-called molecular approach. The real-time scenario of non-Markovian excitation transport due to intra-DOS cascading has been observed in previous femtosecond (fs) fluorescence up-conversion experiments.[12] In accord with the intra-DOS, optical

† Part of the special issure "Harvey Scher Festschrift".
‡ Universität Wien.
§ Philipps-Universität.

10.1021/jp993068d CCC: $19.00
Published on Web 01/15/2000

funneling concept, these studies have demonstrated (i) the pronounced fs red shifts and spectral narrowing of time-windowed fluorescence spectra on time scales up to 2 ps, (ii) the dependence of the fs-decay patterns on the spectral position of the fluorescence probe window, and (iii) the presence of fs-rise terms of low-lying wing states[13] as the natural output of typically sequential exciton population dynamics.[14,15]

Clearly, the time resolution of the above experiments has been not sufficient to directly probe the fate of the initial excitation, rather, these measurements have provided a powerful means to interrogate the asymptotic fs regime of the (incoherent) relaxation. From a first-principle inspection of the problem, one has to conceive that on early time scales the fs pulse couples to the molecular ground and excited state(s) of segmental sites or, more generally, to short-range, spatial domains under definite phase relationships, so a more extended view of excitation transport and transfer in the PPV family must include coherent motion on a short distance and time scale followed by semi-incoherent to pure incoherent coupling events, for longer times. Significantly stronger interactions are expected between strongly coupling segmental units (extended states, weak breaks) than between those segments along the chain that are only weakly coupled (localized states, strong breaks). In particular, for strongly coupling sites within the ensemble of fluctuating site-to-site interactions, the spectrally broad pulse produces miniexcitonic, intersite excitations. The free evolution of these initial coherences is best described in terms of two elementary events: (i) structural relaxation and (ii) electronic intersite coupling, which proceed either simultaneously or via consecutive steps.

While the "sudden" structural reequilibration is the nuclear process that converts the initially bare, elementary site excitation into a dressed state, i.e., the minipolaronic entity, electronic interaction mediated by the neutral, polaron-type miniexciton governs coupled coherent/incoherent motion that degenerates to energy-dispersive hopping on longer fs scales. Thus, to understand the PPV system, one needs information (i) on the nature of the nuclear, motional mode coupled to the $S_1 \leftarrow S_0$ transition and (ii) on the diagonal and off-diagonal elements of the site-energy matrix. Both the nuclear motion (i) initializing the formation of the minipolaronic exciton, and electronic motion (ii) responsible for the intra-DOS energy relaxation (spectral diffusion) give rise to shifts in the frequency space, experimentally observable as a phenomenological Stokes shift between the ground vibrational $S_1 \leftarrow S_0$ and $S_1 \rightarrow S_0$ transitions in absorption and fluorescence, respectively.

II. The Problem

In PPV the overall Stokes shift is small ($\Delta\epsilon \cong 0.15$ eV) and the spectral diffusion ($\Delta\epsilon \cong 0.14$ eV) is exceeding the energy gain of structural relaxation (polaron formation $\Delta\epsilon \cong 0.012$ eV, 100 cm^{-1}).[1,3] The use of an appropriate PPV derivative that exhibits more pronounced nuclear and electronic energy shift terms and thus would allow elucidation of the structural relaxation and electronic coupling matrix elements in a comparative spectroscopic study on PPV is therefore desirable. The present work is intended to investigate the role of both bathochromic shift mechanisms, to figure out their relative orders of magnitude, and to reveal the effect of these couplings on the overall optical dynamics. Variation of the rigidity of the conjugated main chain skeleton in PPV derivatives is a promising tool to elucidate these relaxation pathways. For example, in the ladder-type conjugated polymer poly(*p*-phenylene), LPPP, the extremely rigid backbone of the main chain

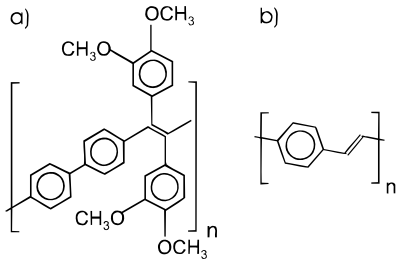

Figure 1. Poly[4,4′-diphenylene-1,2-di(3,4-dimethoxyphenyl)vinylene] DMOP-PDPV (a) and poly(*p*-phenylenevinylene), PPV (b).

prevents nuclear reorientation after electronic excitation, so this system shows, in comparison to PPV, a negligible Stokes shift and excitation transfer behaves nondispersively; that is, the hopping proceeds among energy-degenerate sites in a Markov-type fashion.[16] On the other hand, one would assume a quite different behavior of the optical dynamics for PPV derivatives with flexible main-chain backbones. The polymer under consideration here is poly[4,4′-diphenylene-1,2-di(3,4-dimethoxyphenyl)vinylene), DMOP-PDPV (cf. structure in Figure 1a); a similar component was already studied by stationary, site-selective spectroscopy in the past.[17] As compared to PPV ($\Delta\epsilon \cong 0.15$ eV) and LPPP ($\Delta\epsilon \cong 0.08$ eV), this compound exhibits an enormous overall Stokes shift ($\Delta\epsilon \cong 0.7$ eV) which is caused by the different relative positions of the phenylic rings in the ground and excited state of the biphenyl entity in the main chain. While in the ground state the planes of the phenyl rings are tilted by an angle of about 20°, the planar geometry is predominant in the excited state[17] balanced by a delicate interplay between steric repulsion and the tendency toward extended conjugation.[18] The nuclear rearrangement into the new equilibrium coordinates is executed by an effective torsional motion, so the torsional modes coupled to the electronic Franck−Condon state open up a powerful channel for the structural relaxation process, the latter thereby providing a quite different mechanistic background than that based upon the backbone longitudinal modes in PPV.[17] A second central issue is that the torsional motional modes in the biphenyl repetition units of DMOP-PDPV not only bring about the enhanced Stokes shift, but also reduce, in a second consequence, the spectroscopic overlap integral and, hence, the absolute size of the elementary site-to-site transition rate. As to be demonstrated in this work by fluorescence techniques, one finds, in fact, both the decay and rise terms to be significantly delayed, in comparison to those in the PPV system. The pronounced slowing of the rate of the fluorescence transients in the intermediate relaxation regime is shown to be directly related to the large Stokes shift and thus to a small value of the overlap integral between the absorption and the fluorescence spectrum. The effect of the spectral overlap on the energy transfer parameter of the fluorescence data is indicative of a Förster-type molecule-to-molecule coupling,[19] so the results obtained from the forthcoming studies give further, strong evidence for neutral, *molecular* excitons involved in the energy relaxation.

In this paper fs-fluorescence up-conversion and picosecond (ps) single photon timing will be employed in an attempt to unveil the pathways of torsionally relaxed neutral excitations. These techniques combined with related methods to accumulate gated transient spectra allow collection of high-precision time and frequency domain data over a time scale that ranges from femtoseconds to several nanoseconds. The format of the paper is as follows. In section IVA the optical CW spectra are recapitulated and the transients techniques are described. In section IVB,C a series of temporal and spectral transients is

presented that—due to their slower evolution—provide a unique opportunity to trace the energy loss of relaxing excitonic populations with high accuracy. Included in section IV is a brief remark on the results of transient measurements in the context of analytical theories.[20,21] In section V, a brief theoretical formulation of energy-dispersive hopping is given as a preparatory means to address the nonexponential decay profiles of the DMOP-PDPV fluorescence. Both the Kohlrausch−Williams−Watts target function and the unbiased Laplace inversion are used to fit the distributed fluorescence patterns. A short summary and concluding remarks are given in section VI.

III. Experimental Section

A. Sample Preparation. Poly[4,4-diphenylene-1,2-di(3,4-dimethoxyphenyl)vinylene] (DMOP-PDPV; cf. Figure 1a) is synthesized via dechlorination polymerization of substituted bis-(dichloromethyl)arylene using chromium(II) acetate as the reducing agent ($M_n \gg 3000$ g/mol).[22] The polymer is soluble in various organic solvents such as toluene, chloroform, and chlorobenzene. Transparent films are achieved by casting the polymer from solution on thin microscope slides. Poly(phenylenevinylene) (PPV; cf. Figure 1b) has been used for comparative spectroscopic studies. Its synthesis is based on the sulfonium polyelectrolyte precursor route according to Köpping-Grem et al.[23]

B. Steady-State and Time-Resolved Fluorescence Setups. Absorption spectra were recorded on a Hewlett-Packard 8452A diode-array spectrophotometer (Hewlett-Packard, Palo Alto, CA) using quartz microscope slides. The steady-state fluorescence spectra were recorded on a MPF-44 fluorometer from Perkin-Elmer (Beaconsfield, England). The fluorescence spectra were measured at 4.2 K. A continuous flow liquid helium cryostat (Oxford CF1204, England) was used to control the temperature.

For the picosecond single-photon-counting (SPC) measurements the samples have been excited at 398 nm (3.12 eV) with the second harmonics of a 120 fs laser pulse (fwhm $\gg$ 10 nm) which is generated by an Ar^+-pumped, Kerr-lens mode-locked MIRA 900F Ti:sapphire laser (Coherent, Santa Clara, USA). For the measurement of nanosecond decays the high repetition rate of the MIRA laser (76 MHz) is reduced to 4.75 MHz by inserting a pulse picker (Model 9200, Coherent, Santa Clara, CA) in the beam path in order to prevent multiple excitation events. To exclude scattered light, cutoff filters (GG 420 from Schott, Mainz, Germany) are inserted in the fluorescence path before spectral selection by a single-grating monochromator (Model 1681, Spex, Edison, NJ). Apertures have been adjusted such that, at most, one photon is detected for each exciting event. The signal is detected by a Peltier-cooled MCP 3809U multichannel plate (MCP) from Hamamatsu (Shimokanzo, Japan). The output of the MCP is further processed by conventional SPC modular detection electronics. The picosecond time-resolved spectra were obtained by selecting the desired time window in the multichannel scaling mode of the TAC.

For the detection of femtosecond decay patterns and time-resolved spectra the fluorescence up-conversion technique is applied; details have been given elsewhere.[12] The fundamental of a Ti:sapphire laser (Coherent, Santa Clara, CA) is split on a 20:80 beam splitter. The gate beam (ω_G) passes a variable delay line (Newport Micro Control UT 100.150CC) and is focused onto a 2 mm BBO crystal (cut angle $\alpha = 38°$). The remaining 20% of the original pulse is frequency doubled ($\lambda_{exc} = 398$ nm, 3.12 eV) and used to excite the polymer sample on a spot size of 100 μm diameter. The power of the excitation pulse is reduced to 1 mW and the sample is kept in a vacuum cell to prevent sample degradation. The fluorescence (ω_L) is collected by two off-axis parabolic mirrors with focal lengths of 100 and 150 mm and focused on the BBO crystal, where the sum frequency is generated by type I phase matching ($\omega_{sum} = \omega_G + \omega_L$). The UV sum frequency is filtered by UG11 filters (Schott, Mainz, Germany) and a 22 cm double monochromator (SPEX 1680, 1200 lines holographic grating) and is detected using a photomultiplier (Hamamatsu R 943-02) and standard single channel counting electronics. A 170 fs instrumental response function can be achieved. The crystal phase matching angle, the translation stage, and the data acquisition are computer controlled. The total fluorescence spectra accumulated in distinct gates were spectrally dispersed by the scanning monochromator and corrected for intensity by a computer-controlled feedback loop regulating the optimum (frequency-dependent) phase-matching condition in the nonlinear BBO crystal as a function of the frequency of the fluorescence determined by the position of the rotating monochromator. In the measurement of the fs/early ps up-converted fluorescence photons, the sum-frequency signal S is expressed by

$$S(t) = \int_{-\infty}^{t} F^{\delta}(t')\, C(t-t')\, dt' \qquad (1)$$

F^{δ} is the molecular delta-pulse fluorescence response and C is the measured cross-correlation trace between the excitation pulse scattered from the sample under investigation and the (delayed) probe (gate) pulse at the nonlinear BBO crystal used for fluorescence mixing. Thus no a priori information about the shape of the laser pulse is necessary which offers advantages in the reconvolution of the desired kernel (section IV).

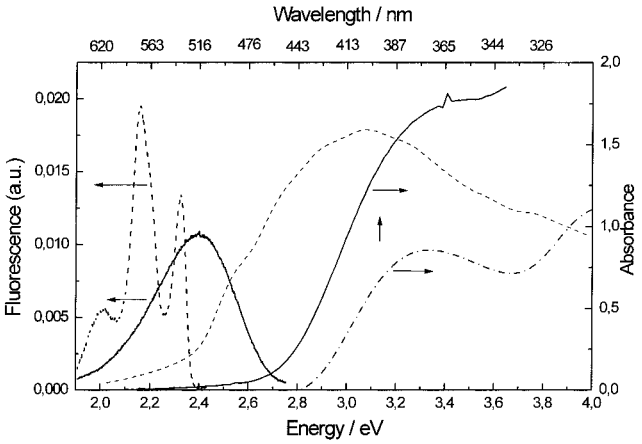

Figure 2. Absorption and fluorescence spectra of DMOP-PDPV of a bulk film (solid curves). Horizontal arrows refer to the fluorescence and absorbance y-axis, respectively. The vertical arrow indicates the position of the excitation energy, $\epsilon_{exc} = 3.12$ eV. The solution spectrum of DMOP-PDPV (dashed−dotted) is also shown. For comparison, absorption and fluorescence of bulk PPV are in dashed lines.

IV. Results and Discussion

A. Steady-State Spectra. The most striking feature of the steady-state absorption and emission spectra of DMOP-PDPV is the huge Stokes shift. In Figure 2 the absorption and emission spectra of DMOP-PDPV (solid curves) along with the solution absorption spectrum (dashed−dotted) are compared with those of PPV (dashed patterns). It becomes evident from the comparison that the spectral overlap of DMOP-PDPV is smaller by more than 1 order of magnitude compared to PPV.

In comparison to PPV, the $S_1 \leftarrow S_0$ part of the absorption spectrum of DMOP-PDPV is hypsochromically shifted and the

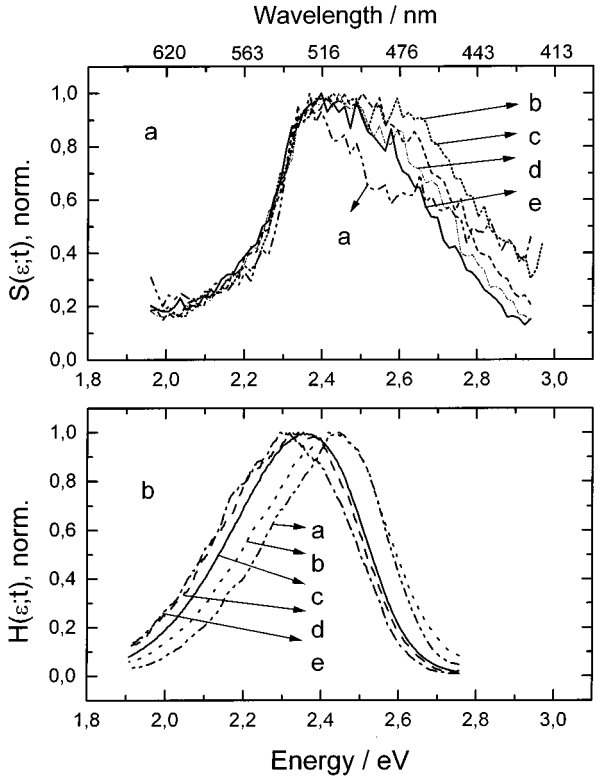

Figure 3. Spectral fluorescence transients in DMOP-PDPV: (a) Scaled up conversion data, temporal range 0−5 ps (a = 0 ps, b = 0.5 ps, c = 2 ps, d = 5 ps) showing spectral narrowing on the blue wing and small shift tendency. (b) Scaled SPT-time-windowed spectra evolving in the intermediate-to-long-time regime of spectral diffusion (a = 50 ps, b = 115 ps, c = 1.5 ns, d = 2.63 ns), e = steady-state spectrum.

red-wavelength trailing edge of the spectrum representing the spectral position of the 0−0 $S_1 \leftarrow S_0$ transition is less steep, which is indicative of a broader distribution of conjugation lengths and thus a larger inhomogeneous bandwidth. Even more striking are the different spectral structures in the patterns of the fluorescence spectra of both polymers. While in PPV the fluorescence bands corresponding to different vibronic transitions in the Franck−Condon (FC) progression are well resolved, only a broad, structureless spectral envolope can be seen in the DMOP-PDPV spectrum. The spectroscopy of biphenylic derivatives is well-known in the literature.[24] In the DMOP-PDPV polymer the vibronic ground level and the set of higher vibrations in the biphenylic segmental sites are, additionally, coupled to low-energetic, torsional modes. This coupling to the torsional modes erodes the discrete transitions and—paralleled by the large inhomogeneity of the transitions—leads to multiline spectral convolutions of nonresolvable transitions and hence to structureless shapes in both absorption and fluorescence (cf. below).

B. Spectral Fluorescence Transients. To track the initial evolution of optical excitations in DMOP-PDPV, the gated fluorescence frequency-mixing technique (see section IIIb) has been employed. The sample has been excited by the second harmonic of the Ti:sapphire laser output ($2\omega_0$, $\epsilon = 3.12$ eV, $\lambda = 397$ nm), the excitation energy thus being within the high-energy tail of the ground-vibrational S_1-state. Under these excitation boundaries we may assume the sudden preparation of the torsional optical excitation to be initially located in the FC space.

Figure 3a displays the sequence of spectrally changing, up-converted fluorescence photon distributions that directly map out the early energy loss of evolving populations on time scales up to 5 ps. The frequency transients display a significant spectral narrowing on the high-energy side but show, on the other hand, a pronounced bottleneck on the red edge; i.e., they are spectrally fixed on the low-energy side and rather invariant in time. Figure 3b shows the spectral fluorescence evolutions of longer lived populations accumulated by SPT measurements, for distinct time windows ranging on a time scale from ≅50 ps to 3 ns. In this regime the central mean value of the spectra is subject to a pronounced energy shift, while the width of the frequency transients remains constant, the early ns-fluorescence lifetime of isolated segmental site units thereby determining the asymptotic regime of energy relaxation.

Due to the special time limits of the fluorescence configurations used in this study, no temporal characterization of the fluorescence spectrum has been available in the 5−50 ps domain. The latter temporal gap would be accessible, for example, in a combination of our methods with streak-camera measurements. Although this intermediate temporal part is lacking, the data are quite satisfactory to allow the overall energy relaxation process to be categorized into roughly three temporal scales. Inspection of the time-windowed patterns a (0 fs) and b (200 fs) in Figure 3a shows that their shapes resemble the stationary one (Figure 2); thus even after this ultrashort delay, the major part of the Stokes shift has already evolved on this time scale. So, quite obviously, the nuclear equilibration subsequent to the FC excitation and driven by some torsional modes takes place on a time scale which is beyond our instrumental resolution (<200 fs).

The second temporal regime after the structural relaxation and proceeding on a time scale up to 5 ps corresponds to, mainly, electronic level relaxations among time-invariant sites (cf. Figure 3a, patterns corresponding to times 0, 0.5, 2.0, and 5.0 ps, respectively). Both the pronounced *spectral narrowing* and the decrease of the central mean of the fluorescence energy strongly indicate energy-dispersive population transfer. Narrowing of the transient fluorescence spectra is, phenomenologically, due to the systematic red shift of the blue wing of the DOS, while the low-energy edge of the spectra remains constant over this relaxation scale. Microscopically, the vanishing blue part of the spectra is the natural output of a migrative release of elementary S_1-excitations starting with the very rapid jumps from the few wing states in the high-energy range of the DOS and reaching lower energy positions, as time proceeds. The red-wavelength bottleneck, however, is the kinetic signature of a migrational blockade, where the hopping transport on the site ensemble stops, that is, intersite excitation transfer is strongly slowed, on this time scale. Consequently, in this special time and energy regime, the residence times of electronic site excitations are increased with regard to those of higher lying states, so the net result is an optical funneling process as displayed by the spectral transients (Figure 3a, curves a−e). Source and gain terms of excitation transfer are not well balanced in dispersive transport; hence the hierarchy of intersite processes gives rise to intermediate excitation funnels in this system. This effect is in particular pronounced in the DMOP system, because the elementary step of excitation transfer is strongly reduced as compared to PPV. Note that recording up-converted fluorescence spectra for time gates >5 ps was not possible in these measurements. Since the lower bound of the SPT technique is ≈40 ps, there was no insight to the continuous ps evolution of the spectra on the time base 5 ps $< t <$ 40 ps.

In the time range 40 ps to 3 ns the typical features of spectral relaxation are observed (Figure 3b). In this time regime the shapes of the fluorescence spectra are time invariant; i.e., the

short-time bottleneck effect (Figure 3a) has been released. Instead, the spectral relaxation continues until the intrinsic fluorescence lifetime of the chain segments is attained. A typical feature of energy-dispersive excitation energy transfer is the decrease of the central mean energy $\langle E \rangle$ of the transient F-spectra, as time proceeds. The spectra sampled at time t map out the average energy of excited-state walkers on their pathways from the center into the tail and bottom states of the DOS. The functional form of the mean-energy relaxation relies on the analytical theory given by Movaghar et al.[20,21] (vide infra).

Further data analysis is complicated by the absorption and fluorescence spectra of a chromophore in which an excitation is coupled to both vibrational and torsional modes thus giving rise to a significant shift of the potential energy profile in the configurational coordinates. Without any inhomogeneous level broadening a $S_1 \leftarrow S_0$ 0−0 transition is followed by a vibrational manifold whose intensity distribution is given by the vibrational Huang−Rhys factor S_v. In addition, each of the transitions is coupled to a manifold of torsional modes of energy $\hbar\omega_t$ whose amplitude is controlled by another Huang−Rhys factor S_t which characterizes the strength of the coupling. As a result, both, the absorption and fluorescence spectra, are more or less structureless and the energy of the adiabatic $S_1 \leftarrow S_0$ 0−0 transition is determined by the common origin of the mirror symmetric spectra. The overall Stokes shift is a measure of the structural relaxation of the chromophore involving vibrational and torsional modes. In the case of inhomogeneous level broadening, for instance, a distribution of adiabatic transition energies, the absorption spectra will show additional band broadening, usually at the low-energy tail. In a bulk system energy transfer will occur leading to spectral relaxation.

The transient fluorescence spectra which have been measured in the experiments are assigned to the vertical transitions, i.e., a Franck−Condon transition from an already vibrationally and torsionally relaxed S_1 excitation. Based upon ref 20, the master curve in Figure 4 shows how the mean energy of an ensemble of random walkers should evolve in time relative to the center of the energy distribution (solid curve). The relaxation energy is normalized to the variance σ of a Gaussian density of states (DOS) distribution. The time axis is set by the nearest neighbor jump time t_h in the absence of disorder. Within the time domain 4 ps to 2.5 ns, a perfect fit between theory and experiment is obtained, based upon the parameter set $t_h = 9$ ps, $\sigma = 0.15$ eV and a vertical transition energy $\langle E^{vert} \rangle = 2.6$ eV within the domain after structural relaxation and commencement of energy transfer. A still acceptable fit is obtained for $\langle E^{vert} \rangle = 2.65$ eV, $t_h = 3.5$ ps, and $\sigma = 0.16$ eV.

The extrapolated value $\langle E^{vert} \rangle$ is in accordance with the high-energy maximum of the fluorescence spectrum at $t = 0$ (Figure 3a). The inferred nearest neighbor jump time is about 1 order of magnitude larger than that of PPV. This is a signature of weaker spectral overlap among absorption and emission due to structural relaxation. As far as the structural energy, i.e., the difference between the adiabatic $S_1 \leftarrow S_0$ 0−0 transition energy and $\langle E^{vert} \rangle$, is concerned we can make a crude estimate based upon the intersection between the low-energy tail of the $S_1 \leftarrow S_0$ transition in solution and the high-energy tail of the $S_1 \rightarrow S_0$ emission at $t = 0$. Ignoring the residual inhomogeneous broadening in solution, the former has to be identified by the disorder free adiabatic $S_1 \leftarrow S_0$ 0−0 transition. From $\langle E^{adiab} \rangle \simeq$ 2.8 eV one arrives at a mean structural energy of 0.2 eV. This value is comparable to a similar poly(biphenylenevinylene) (0.21 eV), in which two phenylene groups are attached to vinylene moiety.[8]

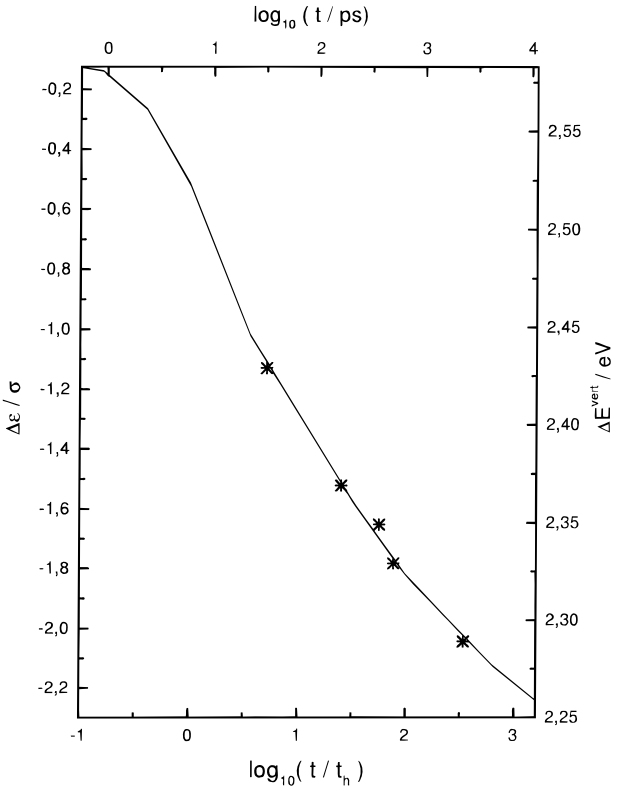

Figure 4. Solid curve: mean relaxation energy $\Delta\epsilon$ of excitations migrating within a Gaussian manifold of hopping sites of variance σ as a function of time, normalized to the nearest neighbor jump time t_h (from ref 20). Stars are the experimental peak fluorescence energies (from Figure 3b; right ordinate and upper abscissa scales have been drawn assuming $\sigma = 0.15$ eV and a vertical transition energy of 2.6 eV at $t \rightarrow 0$.

C. Fluorescence Decays. The significant, bathochromic shifts of the transient F-spectra of DMOP displayed in Figure 3a,b, or, alternatively, the decrease of the mean fluorescence energy $\langle E \rangle$ as time evolves (Figure 4) are strongly indicative of sequential downhill population transfer processes. Therefore, inspection of the energy dissipation process by means of single wavelength fluorescence kinetics should give rise to fluorescence temporal profiles that show pronounced changes with varying spectral positions of the fluorescence probing window.

In Figure 5a the scaled intensities of up-converted F-convolutions of DMOP-PDPV [$S(t;\epsilon)$], including the pulse-to-pulse cross-correlation C (cf. eq 1) are plotted over the probe pulse delay (noisy patterns) for the fluorescence window $\epsilon = 2.69$ eV. Figure 5b shows the evolution of the fluorescence transient detected at $\epsilon = 2.0$ eV and measured over a 80 ps extended scale. The inset displays the fs F-transient of similar low-energy tail states ($\epsilon = 2.25$ eV) in PPV,[12] for comparison.

The fluorescence raw data accumulated for different spectral windows (Figure 5a,b) exhibit different decay rates, the intensity of the decays being lower the more short-lived they are. Again, the decays are significantly slower than those in PPV under comparable conditions,[12] due to the smaller Förster elementary coupling rates, the overall relaxation scale thereby being shifted by approximately 1 order of magnitude to longer times! The solid lines correspond to the best fits based upon exponential target functions that, in a first approach, are intended to parametrize the underlying fluorescence delta-pulse response (cf. eq 1) with the help of an iterative fit-and-compare reconvolution procedure. The pattern in Figure 5a can be fitted to a double-exponential form.

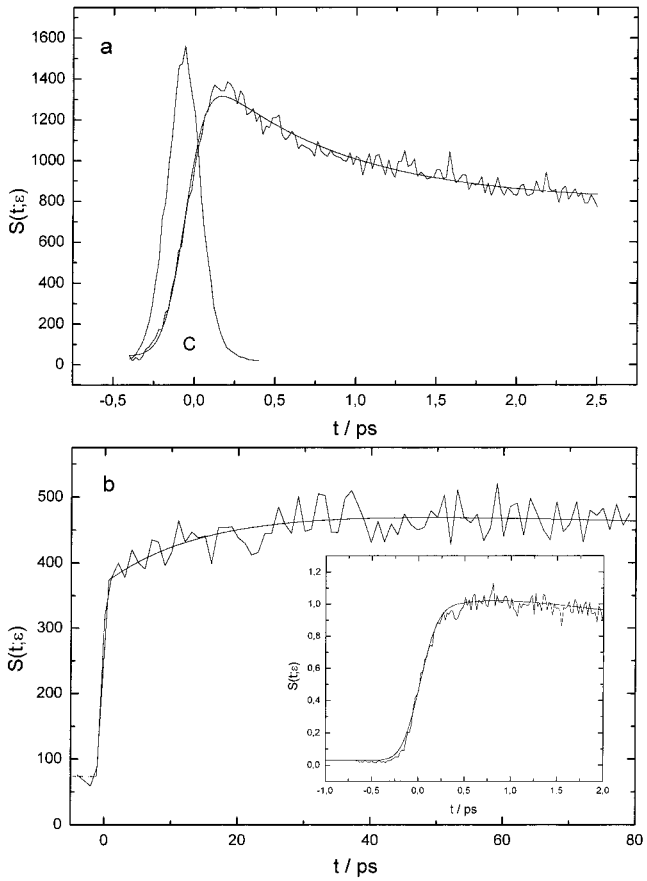

Figure 5. (a) Up-conversion decay patterns at characteristic fluorescence windows, $\epsilon = 2.69$ eV. C, cross-correlation of the excitation pulse: noisy profile, experimental data; solid pattern, best fit (see text for details). (b) Up-conversion fluorescence rise-term at the detection window: $\epsilon = 2.00$ eV. Inset, rise and decay fluorescence patterns of PPV at $\epsilon = 2.25$ eV,[13] for comparison. Note the different time scales in the optical dynamics between DMOP-PDPV and PPV.

A striking result that comes out from the up-conversion studies is the probing of a pronounced *rise* phase for fluorescence photons accumulated in the low-energy window at $\epsilon = 2.0$ eV (Figure 5b). The growth term for low-lying detection windows is, in fact, the kinetic fingerprint of a consecutive process in the tail-state regime, low energetic states thereby being populated and depopulated by (incoherent) excitations cascading through the DOS. The curve maximum is rather flat and requires, at least, a time window of 80 ps base to be detected. Gain and loss of site population in the red edge of the wing states are therefore significantly delayed in DMOP-PDPV, as compared to the extremely rapid serial fluorescence kinetics among energetically similar tail states in PPV (cf. inset, Figure 5b). For the biphenylic polymer the biexponential reconvolution analysis recovers, typically, a rise time $\tau_1 \approx 15$ ps and a decay time $\tau_2 \approx 1.3$ ns, whereas for PPV the same procedure has yielded, in previous investigations,[13] rise times of several hundred fs and decay components $\tau_2 \approx 10$ ps,respectively. The reliability of the τ_1 term reconvolved from the rising edge part (with negative amplitude) clearly, slightly varies depending on whether the slow decay time τ_2 is fixed as a preconceived parameter (from independent SPT measurements) or is processed as a freely floating quantity in the fit optimization process.

In Figure 6 the early time decays of Figure 5a,b have been traced back to the intermediate picosecond and the asymptotic nanosecond scale by employing the SPT technique, while keeping the excitation wavelength ($\lambda_{exc} = 397$ nm, $\epsilon_{exc} = 3.12$ eV) fixed. Figure 6 shows a series of various fluorescence decay

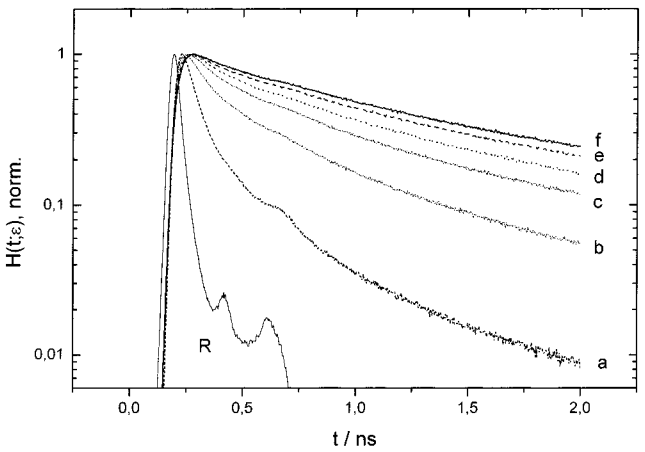

Figure 6. Single wavelength fluorescence kinetics, SPT data in the intermediate-to-long-time relaxation. Decreasing the energy of the detection window results in a slowing of the overall decay: a = 2.76 eV, b = 2.52 eV, c = 2.37 eV, d = 2.25 eV, e = 2.07 eV, f = 1.91 eV, R = instrumental response.

patterns in a semilogarithmic plot detected at ϵ: a = 2.76 eV, b = 2.52 eV, c = 2.37 eV, d = 2.25 eV, e = 2.07 eV, and f = 1.91 eV, respectively, and ranging from approximately 40 ps up to a few nanoseconds. Qualitatively, the rates of the SPT fluorescence decays drop rapidly with increasing energies of the probing window which is in accord with the behavior in the early ps regime (Figure 5a,b). The high-precision data patterns (10^5 in the peak channel) relax over more than three decades and exhibit, quite evidently, highly nonexponential behavior. In a first approach to parametrizing the profiles, three- or four-exponential target functions have been used in the reconvolution fit procedure. Further, for the entire set of profiles, only positive amplitudes and thus decaying components have been extracted by the routines, the reliability of 15 ps rise terms made possible by up-conversion (cf. above), being a critical enterprise in the SPT technique.

V. Theoretical Excourse—Nonexponential Fluorescence

As the experiments have demonstrated, the fluorescence in DMOP-PDPV is the natural output of an electronically excited, segmental site ensemble with pronounced self-energy (diagonal) disorder and a fluctuation of site-to-site transitions. As a consequence, the data profiles in Figure 6 have to be considered as the typical fingerprint of dispersive fluorescence kinetics. Following previous, systematic work in this field,[14] the average fluorescence response after uniform delta-pulse population of the (structurally relaxed) S_1 -DOS, for a distinct subensemble of segmental sites collected in a spectral window at ϵ (with width $\Delta\epsilon$), can be expressed as the factored result of a radiative and a statistical mechanical probability term

$$F^{\delta}(t;\epsilon) \propto \mathrm{e}^{-t/\tau_0} \langle p(t;\epsilon) \rangle \tag{2}$$

Here the exponential decay spans up the radiative part with τ_0 being the intrinsic fluorescence lifetime of an isolated, segmental (monomeric) subunit, while $\langle p(t;\epsilon) \rangle$ denotes the segmental donor site survival probability

$$\langle p(t;\epsilon) \rangle = \int_0^{\infty} \langle \Phi(\lambda;\epsilon) \rangle \mathrm{e}^{-\lambda t}\, \mathrm{d}\lambda = \hat{L} \langle \Phi(\lambda;\epsilon) \rangle \tag{3}$$

expressed in terms of the Laplace transform $\hat{L}$ of the underlying spectrum of hopping modes $\langle \Phi(\lambda;\epsilon) \rangle$ for $N \rightarrow \infty$ statistically independent single chain configurations, with λ being the (positive) eigenvalues of the down-chain excitation hopping

processes. Both the λ_i's and the corresponding eigenvectors Φ_i of the many-body site-to-site transfer in a single chain result from the diagonalization of a high-dimensional asymmetric energy-space master equation[12,14]

$$\dot{p}(t) = W(\{\epsilon_i | i = 1, ..., n_D\}, \{r_i | i = 1, ..., n_D\})\, p(t) \quad (4)$$

$$W = [w_{ij}]_{n_D \times n_D}; \quad w_{ij} = \chi(r_{ij})\, \theta(\epsilon_i, \epsilon_j)$$

with elements w_{ij} of the excitation relaxation matrix **W** containing the distance, $\chi(r_{ij})$, and energy-dependent transition probabilities $\theta(\epsilon_i,\epsilon_j)$.[14]

The space-dependent term in the above expression of the hopping rates between segmental donor sites, w_{ij}, has the Förster type form

$$\chi(r_{ij}) = n_0 \left(\frac{d}{|r_i - r_j|} \right)^6 \quad (5)$$

while the energy factor is described by a Boltzmann-type balance equation

$$\theta(\epsilon_i,\epsilon_j) = \begin{cases} \exp[-(\epsilon_j - \epsilon_i)/kT], & \epsilon_j > \epsilon_i \\ 1, & \epsilon_j \le \epsilon_i \end{cases} \quad (6)$$

This ansatz used in several studies[12,14] accounts for thermally activated uphill jumps and downhill hopping among energetically different donor sites that are assumed to be energy- and time-invariant. Note that this incoherent approach, clearly, leaves no room for the initial coherence of miniexcitonic site excitations (cf. the coherent scenario, section VI).

The hopping modes λ are inversely related to the lifetime space, $|\lambda| = (1/\tau) - (1/\tau_0)$, so eqs 2 and 3 are equivalent to

$$F^{\delta}(t;\epsilon) \propto e^{-t/\tau_0} \int_0^{\infty} \langle \Phi(\tau,\epsilon) \rangle e^{-t/\tau}\, d\tau =: \hat{L}\langle \Phi(\tau;\epsilon,\tau_0) \rangle \quad (7)$$

A. The Kohlrausch−Williams−Watts Function. Although conceptually simple, the strict microscopic description of energy-dispersive hopping in diagonally disordered molecular systems is especially complex. Since the elementary excitation is preferentially transported in the direction of lower energies, one is confronted with the problem that (i) spatial transport is coupled to energy relaxation, (ii) the density numbers of transport states represent a temporally variable quantity, and (iii) the evolution depends on the energy of the originally excited state in the density distribution. Considerable advance was made, in the past, in particular, by Movaghar et al.,[20,21] who analyzed the nonequilibrium, transport Green solution to the master equation (eq 3) in terms of an analytic effective medium approximation and, very recently, by Vissenberg[15] in systematic work using the Green site formalism with special emphasis placed on the carrier- and optical dynamics in conjugated polymers.[25] In general, these solutions involve complicated series expansions and numerical integrals in the Laplace domain, so their use as target functions in the context with the ill-posed inverse Laplace transform is questionable and, in most cases, not tractable with satisfactory precision in the deconvolution analysis of fluorescence profiles. Time-domain approximations to the Laplace Green function solution provide, therefore, an important alternative to make nonexponential fluorescence analysis in many-body systems more reliable. For dipolar coupling and distinct transport dimensionalities the time-domain, stretched exponential form of the Kohlrausch−Williams−Watts (KWW) relaxation type[26] has been demonstrated, in the past, to be the analytical result from the two-body cumulant approximant[27] for an infinitely disordered system with *degenerate* site energies. However, the generality and the widespread use of the law in different areas of relaxation physics have, meanwhile, indicated that the KWW function is, by no means, specific, but rather reflects the distributed nature of microscopic relaxations in disordered materials, in general. While the extended exponential is associated with a picture of parallel (i.e., unconstrained) relaxation,[28−30] it has been shown to belong to a quite general class of hierarchically constrained models[31−33] as well, including the sequential multistep models in the target[34,35] and trapping problem,[36] with the aid of both fractal[37,38] and CTRW concepts.[39−41]

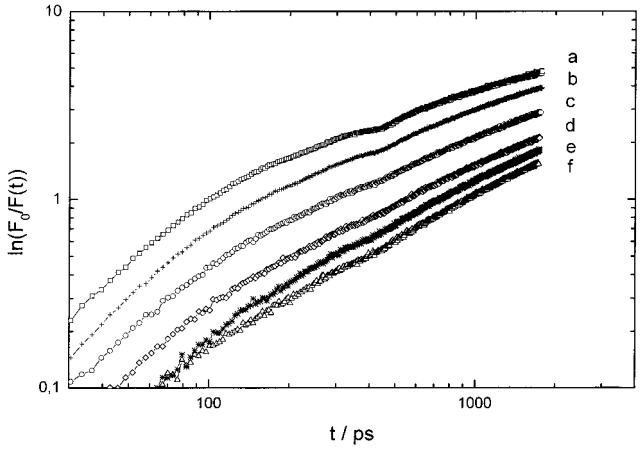

Figure 7. Linearized KWW plots of SPT fluorescence transients, data from Figure 6. Pronounced deviations, formally equivalent to a time-dependent dispersion parameter α (t). Trends to monoexponential decays at early times, tendency toward constant α in the asymptotic range. See discussion in the text.

The latter serial relaxation models[34−38] are, mechanistically, closely related to energy-dispersive hopping in DMOP−PDPV; consequently, it is tempting to conjecture that our energy-dependent (delta-pulse) fluorescence profiles convolved in the raw data of Figure 6 satisfy the stretched exponential form—a procedure that was used, previously, in the analysis of polymer fluorescence anisotropy data.[42,43] In our case we use the energy-selective KWW response

$$F^{\delta}(t;\epsilon) \propto \exp\left(-\left(\frac{t}{t_0'} \right)^{\alpha} \right) \quad (8)$$

which is a theoretically sound result[44] for energy-transfer systems with static site-energy disorder. α describes the dispersion and $t_0' = t_0\gamma(\epsilon)$ is the product of a spatial and energy-dependent quantity that spans-up the time-base of relaxation. A direct forward reconvolution based upon the KWW-target function (eq 8) with α, t_0', and the prefactor freely varying in iterative fit-and-compare cycles yielded significant correlations and unacceptable fits. Thus, in order to examine the validity of the KWW expression, the reconvoluted, multiexponential delta-pulse fluorescence data (Figure 6) have been replotted with relaxation scales covering more than three decades and a time resolution close to 30 ps. Due to the unsatisfactory quality of the fluorescence up-conversion early-ps data, these patterns have not been considered in the following fit procedures.

The linearized KWW plots—logarithmic plots of $\ln(F_0/F(t))$ versus t—for various detection windows set at a = 2.76 eV, b = 2.64 eV, c = 2.52 eV, d = 2.37 eV, e = 2.25 eV, and f = 2.07 eV, respectively, are shown in Figure 7. In all cases the experimental F-profiles at intermediate times strongly deviate

from the KWW form. For early times up to 60 ps, in particular, the high-energy profiles f and e approach the slope $\alpha \sim 1$. This is the limit of vanishing dispersion and thus the signature of an exponential decay. In the context of the hierarchical structure and the nonergodicity of this special class of energy transfer, the qualitative understanding of these results is straightforward. At short times and for spectral detection windows in the range of the high-energy tail states, the relaxation is governed by nearest neighbor jumps among an average subensemble of sites given by a maximum coordination number for which the first order decay process is the natural output. For moderate times the probability that a site next to it is lower in energy decreases, and consequently, this is the (blurred) onset of non nearest neighbor jumps that leads to nonexponential contributions to the fluorescence decay in the lower energy regime. For the longer, intermediate times, in the neighborhood of the red-edge states (2.07 eV), transitions from nearest to non nearest site-to-site coupling dominate the decay, with an expectation value of the hopping rate that is time-dependent, $\langle\lambda(t)\rangle$, and hence responsible for the pronounced deviations (curved regions) from the KWW form (Figure 7). In the asymptotic limit where the multistep energy flow tends to be terminated and, predominantly, single-step energy transfer and irreversible trapping proceed among a few, almost isoenergetical sites, a KWW-like behavior with constant exponents near $\alpha \approx 1/2$ emerges. The slope of the curve gradually goes from a value of 0.43 for 2.76 eV (curve f) to 0.66 for 2.07 eV (curve a). The slight deviations from $\alpha = 1/2$ reflect the nonrandom distribution of sites and the finite-size effect in conjugated polymers, but note that, presumably, the asymptotic limit is not fully reached, due to the small overlap integral in the elementary site-to-site transfer among DMOP-PDPV segments. In this case, the fluorescence lifetime $\tau_0 \sim 1$ ns of a monomeric, isolated unit is a natural cutoff.

B. Laplace Inversion of Fluorescence Data. In the preceding section dispersive EET and its typical, time- and energy-dependent features have been demonstrated only indirectly on the basis of a formal time dependence of the KWW dispersion parameter, $\alpha(t)$. Due to the lack of appropriate time-domain target functions, a theoretically sound and rather unbiased fashion is to tackle directly the distributions of hopping modes $\langle\Phi(\tau;\epsilon)\rangle$ and their temporal change along the energy-relaxation coordinate by inverting the ps-SPT data of Figure 6 with the help of the exponential series method (ESM).[45,46] We have applied the numerical technique to the analysis of synthetic data[14,48] and, in preliminary, real-time experiments, to the intermediate fluorescence relaxation regime in PPV.[12] Meanwhile, the routines have become more stable and hold promise as the method of choice in the extraction of $\langle\Phi(\tau,\epsilon)\rangle$. Briefly, in the fluorescence raw-data convolution H [$R(t)$, laser excitation SPT response]

$$H(t;\epsilon) \equiv R(t) \otimes F^{\delta}(t;\epsilon) \equiv R(t) \otimes \hat{L}\langle\Phi(\tau;\epsilon,\tau_0)\rangle \qquad (9)$$

ESM approximates the Laplace transform

$$\hat{L}\langle\Phi(\tau;\epsilon,\tau_0)\rangle \approx \sum_{m=1}^{M} \Phi_m' \, \mathrm{e}^{-t/\tau_m} \qquad (10)$$

in terms of a coarse discretization and reconstructs for a fixed set of τ_m-values (logarithmically distributed along the relaxation scale) approximate, discrete amplitudes Φ_m' in iterative, nonlinear free parameter optimization cycles; thereby the routines are mimicking a sequence of Laplace inversion $\widehat{L^{-1}}$ and deconvolution (operator $\widehat{C^{-1}}$)

$$\widehat{L^{-1}}\,\widehat{C^{-1}}H(t;\epsilon) \rightarrow \hat{L}\langle\Phi(\tau;\epsilon,\tau_0)\rangle \qquad (11)$$

via iterative, *forward* convolution cycles to minimize the expression

$$H(t_k) - \left[\sum_m \Phi_m' \left(\sum_{j=1}^{k-1} R_j \, \mathrm{e}^{-(t_k - t_j)/\tau_m}\right) + \frac{1}{2} R_{\mathrm{K}}\right] \rightarrow \mathrm{MIN} \qquad (12)$$

The second term in eq 12 describes the discretized form of the convolution integral (eq 9), with $H(t_k)$ denoting the experimental fluorescence intensity at time t_k. A Tikhonov regularization[47] function has been used in the minimization procedure; details of the functional have been given elsewhere.[48] The resulting spectra $-m$ amplitudes versus m lifetimes$-$ $\{\Phi_m', \tau_m; \tau_0\}_\epsilon$, represent well-behaved approximations to the exact spectrum of eigenvalues $\langle\Phi(\tau;\epsilon,\tau_0)\rangle$.

The results of the reconvolution-based inversion are displayed in Figure 8. The patterns directly show the distribution of hopping modes in the inverse fluorescence lifetime space $\tau_m \approx 1/\lambda_m < \tau_o$ and are a replica of the relaxational history of optical excitations for times longer than 30 ps. Due to the 30 ps limit in the time resolution of the SPT data, the initial trial inputs (rectangular shapes, i.e., equally weighted amplitudes to prevent preconceived bias) have been constrained to positive amplitudes only; thus the optimized distributions contain, per definition, no rise terms. In fact, the growth term extractable from up-conversion measurements at low energies reaches its maximum near 40 ps (Figure 5b), so its contribution to the SPT data is marginal and negligible, also from the experimental point of view. The spectra span up a time scale ranging from >30 ps up to 1000 ps for fluorescence windows, from top to the bottom: $\epsilon = 2.76$, 2.70, 2.64, 2.58, 2.52, 2.43, 2.37, 2.25, 2.07, and 1.91 eV, respectively. It can be seen that time range, intensity, width, and shape of $\{\Phi_m', \tau_m; \tau_o\}_\epsilon$ strongly depend

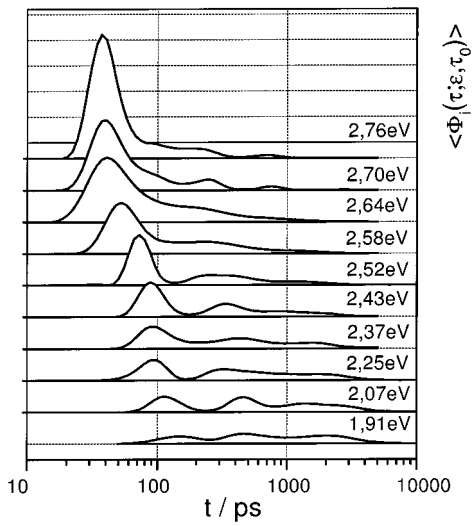

Figure 8. Results of ESM analysis: numerical Laplace inversion that gives rise to the reconstruction of distributions of fluorescence lifetimes $\langle\Phi(\tau;\epsilon,\tau_0)\rangle$ (eq 7), equivalent to the distribution of hopping modes for times $\ll\tau_0$: $\langle\Phi(\lambda;\epsilon)\rangle$ (eq 3). ESM analysis yields the discrete set of amplitude$-$lifetime pairs, $\{\Phi_m',\tau_m;\tau_0\}_\epsilon$ as an approximation to the exact expressions $\langle\Phi(\tau;\epsilon,\tau_0)\rangle$. $\{\Phi_m',\tau_m;\tau_0\}_\epsilon$ demonstrates snapshots of the spectral diffusion. Time and energy dependence of the hopping mode distribution. As time proceeds, the excitation dwell times shift to longer times and low frequency hopping modes get populated in the course of intra-DOS downhill relaxation. Note the tendency toward eroding the initial population of modes, from top to bottom.

on the spectral position of the segment subensemble. Generally, with decreasing energy of the fluorescence window the lifetime spectra, equivalent to the dispersion of hopping modes, are systematically shifted to longer ps times. The lower the energetic position of the fluorescence window, the more pronounced the temporal shift of the central mean, proportional to the expectation value of the hopping rate $\langle\lambda(t)\rangle$.

These novel results obtained by the ESM method thus demonstrate an entirely new platform in probing the spectral diffusion process. The energy dependence of hopping modes associated with their temporal change on ps scales is the most direct, kinetic signature of dispersive excitation transfer that, clearly, goes beyond the fingerprints found in terms of the strong deviations from the linearized KWW function (Figure 7). One readily realizes the physical scenario behind the sequence of distributions. At the high-energy edge of fluorescence detection, $\approx$2.76 eV, larger hopping rates (higher frequency modes) dominate the sub-100 ps range centered around $\tau \approx 50$ ps. This is a consequence of the large number of energetically lower lying segmental sites that act as acceptors in dipolar site-to-site coupling (gain terms), with regard to the energetic slices of higher lying, segmental donor subensembles (loss terms). The temporal shift of the distributions detected at different locations on the energy-relaxation coordinate directly reveals the spreading of the initial $\epsilon = 2.76$ eV population and transfer couplings in the energy matrix. The short-time peak of the high-energy distribution gets eroded and long lifetimes (low-frequency modes) emerge when the detection window is shifted through the DOS, from 2.76 eV down to the tail states at 1.91 eV. The excitation transfer modes evolve over a broad time range and, gradually, smear out and lose structure. However, note that the temporal shift is not paralleled by a substantial narrowing of the lifetime distribution as one would expect in an optical funneling process, due to the delicate interplay between nonradiative, long-range couplings and the intrinsic cutoff made-up by the $\sim$1 ns-fluorescence lifetime.

VI. Summary and Concluding Remarks

In this work fluorescence up-conversion, ps-photon-timing (SPT), and numerical data inversion have been employed in our efforts toward elucidating the nature of photoexcitations in the π-conjugated polyarylene poly[4,4′-diphenylene-1,2-di(3,4-dimethoxyphenyl)vinylene], DMOP-PDPV. Our main concern has been with studying the large, bathochromic Stokes shift of fluorescence and, in particular, quantifying the photophysical scenario of nuclear−electronic relaxation that is consistent with this energy shift. The up-conversion measurements have made it possible to delineate the temporal coordinates of the structural relaxation process ($<$200 fs) and to track the very early stage of energy relaxation ($>$200 fs) that emerges after nuclear equilibration from the high-energy tail of a DOS of fluorescent S_1-levels. Gated, spectral transients have been recorded up to 5 ps (Figure 3a), while in single-wavelength fluorescence detection ultrafast decays of high-energy subensembles (Figure 5a) and pronounced rise terms for low-energy site arrays on extended ps scales have been monitored (Figure 5b). In combination with SPT high-precision ps-data sets—both frequency and time resolved—have been collected that allowed to trace the cascading excitations down to the nanosecond scale (Figure 3b, Figure 6). The mechanism underlying the excited-state energy flow, i.e., the time-variant central mean of total fluorescence energy $\langle E\rangle$ in Figure 4, is dispersive excitation hopping transfer among diagonally disordered, static segmental sites in the DMOP-PDPV polymer, similar to those in the PPV family, but with strongly reduced elementary rates, due to the small overlap integrals between absorption and fluorescence spectra from vertical and structurally relaxed excitation states (Figure 2).

The retardation of the elementary transfer processes in DMOP-PDPV has opened a unique opportunity of measuring dispersive hopping over several relaxational decades and testing Movaghar's theory of spectral relaxation in a quantitative fashion. A particular advantage of a system featuring structural relaxation via coupling to torsional modes is that overlap between absorption and fluorescence is minimized. This eliminates fluorescence reabsorption, notably upon recording the fluorescence decay under conditions of site-selective excitation. This is the reason why in PPV the experimentally recovered spectral relaxation on a ps scale is underestimated.[49] More fundamentally, the successful fit of spectral relaxation in terms of random walks in a rough energy landscape[20] proves that the microscopic process is solely governed by Förster-type coupling, irrespective of the excitation being dressed by a structural relaxation ("exciton polaron" formation) or not as it is in PPV. The distinguishing quantity is the spectral overlap integral which controls the coupling strength and time domain in which transport proceeds.

Another important aspect of the DMOP-PDPV transport system is that the deceleration of the individual segmental site−site transitions has made the accumulation of excitonic fluorescence more reliable. The high-quality SPT data have allowed therefore analysis of a type of nonexponentiality that strongly deviates from the usual KWW stretched exponential form (Figure 7). Based upon a microscopic, energy-dispersive transport model (section V, eq 4) including diagonal site-disorder, off-diagonal, dipolar fluctuations, and a density of states of molecular site excitations, the energy-selective fluorescence responses ($H(t;\epsilon)$, eq 7) in Figure 6 have been analyzed in a specific real-data application of previous computational experiments[48] by means of an iterative reconvolution-based Laplace inversion (eqs 8−12). Energy- and time-dependent distributions of fluorescence lifetimes, equivalent to the dispersion of hopping modes extracted from this procedure (Figure 8), represent a novel approach, in polymer photophysics, to revealing dynamical information from optical relaxation data.

To close this work we note that the time resolution of the fluorescence up-conversion apparatus ($\sim$200 fs) has not been good enough to probe the primary stages of electronic/nuclear motion prior to incoherent dispersive hopping. Therefore, while there is clear evidence from our data that the major part of the initial excitation in DMOP-PDPV evolves on moderate time scales among a long-range disorderd segmental array, our experiments cannot account for the fate of the original Franck−Condon polarization. On early fs scales the scenario is naturally more complex: this regime has extreme boundaries and is initially controlled by the imprinting of phase coherence from the field onto the molecular states of the polymer.[50] Therefore, the new generation of 20 fs excitation and probing pulses[51] will provide a powerful, new tool for precisely this regime! The novel perspective of a 20 fs excited-state excitation for a conjugated polymer is that the extremely broad pulse prepares an ensemble of miniexcitonic, intersite excitations, probably, in their vibrational overtones. The free evolution of the initial coherence is then best described in terms of a complex vibrational wave packet motion which interferes with the structural relaxation of the bare, delocalized intersite excitations into the dressed states of minipolaronic entities. The enormous impact of these pulses is two-fold. (i) We anticipate that the donor coherences of the segmental minibands can be probed

by high-resolution three-pulse photon-echo techniques using 20 fs excitation pulses. The pulses are broad enough to completely cover the large, spectral width of the inhomogeneous $S_0 \rightarrow S_1$ transition in the polymers. Analysis of the (modulated) echo decays may provide access to the pathway of structural relaxation and (small) polaron−exciton formation on time scales <200 fs. (ii) It is tempting to conjecture that the "sudden" structural change in conjugated polymers can be probed from the perspective of the accepting nuclear modes of the polymer environment, in complementary optical-pump−THz-probe experiments.[52] Such future measurements may have the potential to open a new regime in the femtochemical physics of gap states in conjugated polymers.

Acknowledgment. This work was supported by the Austrian Science Foundation (P-12566 PHY) and the Volkswagenstiftung (H.B., project I/71937 "Photonik"). The DMOP-PDPV, poly-[4,4-diphenylene-1,2-di(3,4-dimethoxyphenyl)vinylene] is a gift of Prof. H. H. Hörhold (Friedrich-Schiller-Universität, Jena), who is gratefully acknowledged as is Chan Im for the measurement of the solution spectrum.

References and Notes

(1) Rauscher, U.; Bässler, H.; Bradley, D. D. C.; Hennecke, M. *Phys. Rev. B* **1990**, *42*, 9830.
(2) Pakbaz, K.; Lee, C. H.; Heeger, A. J.; Hagler, T. W.; McBranch, D. *Synth. Met*. **1994**, *64*, 295.
(3) Bässler, H.; Gailberger, M.; Mahrt, R. F.; Oberski, J. M.; Weiser, G. *Synth. Met*. **1992**, *49*−*50*, 341.
(4) Special Issue of *Chemical Physics on Excited-State Phenomena in Conjugated Polymers*; Bässler, H., Rothberg, L. J., Eds.; 1998; Vol. 227.
(5) Su, W. P.; Schrieffer, J. R.; Heeger, A. J. *Phys. Rev. Lett.* **1979**, *42*, 1698.
(6) Lee, C. H.; Yu, G.; Heeger, A. J. *Phys. Rev. B* **1993**, *47*, 15543.
(7) Vardeny, Z.; Ehrenfreund, E.; Brafman, O.; Novak, H.; Schaffer, H.; Heeger, A. J.; Wiedl, F. *Phys. Rev. Lett.* **1986**, *56*, 671.
(8) Gailberger, M.; Bässler, H. *Phys. Rev. B* **1991**, *44*, 8643.
(9) Frankevich, E. L.; Lymarev, A. A.; Sokolik, I.; Karasz, F. E.; Blumenstengl, S.; Baughman, R. H.; Hörhold, H. H. *Phys. Rev. B* **1992**, *46*, 9320.
(10) Bässler, H.; Schweitzer, B. *Acc. Chem. Res.* **1999**, *32* (2), 173.
(11) Yan, M.; Rothberg, L. J.; Papadimitrakopoulos, F.; Galvin, M. E.; Miller, T. M. *Phys. Rev. Lett.* **1994**, *72*, 1104. Yan, M.; Hsieh, B. R.; Alfano, R. R. *Phys. Rev. B* **1994**, *49*, 9419.
(12) Mollay, B.; Lemmer, U.; Kersting, R.; Mahrt, R. F.; Kurz, H.; Kauffmann, H. F.; Bässler, H. *Phys. Rev. B* **1994**, *50* (15), 10769. Kersting, R.; Mollay, B.; Rusch, M.; Wenisch, J.; Leising, G.; Kauffmann, H. F. *J. Chem. Phys.* **1997**, *106*, 2850.
(13) Warmuth, Ch.; Tortschanoff, A.; Brunner, K.; Mollay, B.; Kauffmann, H. F. *J. Lumin.* **1998**, *76*, 498.
(14) Mollay, B.; Kauffmann, H. F. Dynamics of Energy Transfer in Aromatic Polymers in Disorder Effects on Relaxational Processes; Richert, Blumen, Eds.; Springer-Verlag: New York, 1994.
(15) Vissenberg, M. C. J. M. Opto-Electronic Properties of Disordered Organic Semiconductors. Thesis, Leiden, 1999; Chapter 5.
(16) Mahrt, R. F.; Pauck, T.; Lemmer, U.; Siegner, U.; Hopmeier, M.; Hennig, R.; Bässler, H.; Göbel, E. O.; Haring-Bolivar, P.; Wegmann, G.; Kurz, H.; Scherf, U.; Müllen, K. *Phys. Rev. B* **1996**, *54*, 1759.
(17) Mahrt, R. F.; Bässler, H. *Synth. Met*. **1991**, *45*, 107.
(18) Lowry, T. H.; Schueller-Richardson, K. *Mechanism and Theory in Organic Chemistry*; Harper Collins Publishers: New York, 1987.
(19) Förster, T. *Z. Naturforsch*. **1949**, *4a*, 321.
(20) Movaghar, B.; Grünewald, M.; Ries, B.; Bässler, H.; Würtz, D. *Phys. Rev. B* **1986**, *33*, 5545.
(21) Movaghar, B.; Ries, B.; Grünewald, M. *Phys. Rev. B* **1986**, *34*, 5574.
(22) Hörhold, H.; Helbig, M. *Makromol. Chem., Macromol. Symp.* **1987**, *12*, 299.
(23) Köpping-Grem, G.; Leising, G.; Schmetta, M.; Stelzer, F.; Huber, A. *Synth. Met.* **1996**, *76*, 53.
(24) Bridges, J. W.; Creaven, P. J.; Williams, R. T. *Biochem. J.* **1965**, *96*, 872.
(25) Vissenberg, M. C. J. M.; de Jong, M. J. M. *Phys. Rev. Lett.* **1996**, *77*, 4820; *Phys. Rev. Lett.* **1997**, *78*, 4302.
(26) Williams, G. *Adv. Polym. Sci.* **1979**, *33*, 59.
(27) Huber, D. L. *Phys. Rev. B* **1979**, *20*, 2307.
(28) Klafter, J.; Blumen, A. *Chem. Phys. Lett.* **1985**, *119*, 377.
(29) Klafter, J.; Shlesinger, M. F. *Proc. Natl. Acad. Sci. U.S.A.* **1986**, *83*, 848.
(30) Soules, T. F.; Markovsky, A. *J. Chem. Phys.* **1987**, *86*, 5874.
(31) Palmer, R. G.; Stein, D. L.; Abrahams, E.; Anderson, P. W. *Phys. Rev. Lett.* **1984**, *53*, 958.
(32) Bendler, J. T.; Shlesinger, M. F. *Macromolecules* **1985**, *18*, 592.
(33) Ngai, K. L.; Rajagopal, A. K.; Teitler, S. *J. Chem. Phys.* **1988**, *88*, 5086.
(34) Blumen, A.; Zumofen, G.; Klafter, J. *Phys. Rev. B* **1984**, *30*, 5379.
(35) Montroll, E. W.; Bendler, J. T. *J. Stat. Phys.* **1984**, *34*, 129.
(36) Blumen, A.; Zumofen, G.; Klafter, J. *J. Stat. Phys.* **1984**, *36*, 533.
(37) Klafter, J.; Blumen, A. *J. Chem. Phys.* **1984**, *80*, 875.
(38) Blumen, A.; Klafter, J.; Zumofen, G. in *Optical Spectroscopy of Glasses*; Zschokke-Gränacher, I., Ed.; Reidel: Dordrecht, 1986; p 199.
(39) Montroll, E. W. *J. Math. Phys.* **1969**, *10*, 753.
(40) Scher, H.; Lax, M. *Phys. Rev. B* **1973**, *7*, 4491; *Phys. Rev. B* **1973**, *7*, 4502.
(41) Scher, H.; Montroll, E. W. *Phys. Rev. B* **1975**, *12*, 2455.
(42) Peterson, K. A.; Fayer, M. D. *J. Chem. Phys.* **1986**, *85*, 4702.
(43) Baumann, J.; Fayer, M. D. *J. Chem. Phys.* **1986**, *85*, 4087.
(44) Mollay, B.; Kauffmann, H. F. *J. Chem. Phys.* **1992**, *97*, 4380.
(45) Landl, G.; Langthaler, T.; Engl, H. W.; Kauffmann, H. F. *J. Comput. Phys.* **1991**, *95*, 1.
(46) James, D. R.; Ware, W. R. *Chem. Phys. Lett.* **1986**, *126*, 7. Siemarczuk, A.; Ware, W. R. *J. Phys. Chem.* **1989**, *91*, 3677.
(47) Tikhonov, A.; Arsenin, V. *Solutions of ill-posed problems*; Wiley: New York, 1977. *Inverse and ill-posed problems*; Engl, H. W., Groetsch, C. W., Eds.; Academic Press: New York, 1987.
(48) Mollay, B.; Kaufmann, H. F. *Chem. Phys*. **1993**, *177*, 645.
(49) Kersting, R.; Lemmer, U.; Mahrt, R. F.; Leo, K.; Bässler, H.; Göbel, E. O. *Phys. Rev. Lett.* **1993**, *70*, 3820.
(50) Mukamel, S.; Tretiak, S.; Wagersreiter, T.; Cherniak, V. *Science* **1997**, *277*, 781.
(51) For example: *Ultrafast Phenomena XI*; Elsaesser, T., Fujimoto, J. G., Wiersma, D. A., Zinth; W., Eds.; Springer Series in Chemical Physics; Springer: New York, 1998; Part I.
(52) McElroy, R.; Wynne, K. *Phys. Rev. Lett.* **1997**, *79*, 3078. Kersting, R.; Unterrainer, K.; Strasser, G.; Kauffmann, H. F.; Gornik, E. *Phys. Rev. Lett.* **1997**, *79*, 3038.